View Online

Doping strategy of carbon nanotubes with redox chemistry†

Ki Kang Kim,[a] Seon-Mi Yoon,[b] Hyeon Ki Park,[a] Hyeon-Jin Shin,[ab] Soo Min Kim,[a] Jung Jun Bae,[a] Yan Cui,[a] Jong Min Kim,[b] Jae-Young Choi*[b] and Young Hee Lee*[a]

Received (in Gainesville, FL, USA) 21st February 2010, Accepted 1st June 2010
DOI: 10.1039/c0nj00138d

The chemical doping of single-walled carbon nanotubes (SWCNTs) has been an important issue in tailoring the electronic structures of SWCNTs. This paper proposes a strategy for controlling the doping types and doping concentrations by choosing the reduction potential of a dopant relative to the redox potential of SWCNTs. For this purpose, the redox potential plot in terms of the chirality and diameter was generated based on theoretical calculations, which were in good agreement with the experimental data obtained from individually separated SWCNTs. The change in the electronic structures of the SWCNTs with the various dopants was clearly observed by absorption and Raman spectroscopy, and was explained well by the redox potential argument. This principle was tested further by fabricating transparent conducting films followed by doping. Doping with Au^{3+} resulted in a sheet resistance of 100 Ω sq^{-1} at 90% transmittance. This SWCNT doping strategy for both n-type and p-type materials can be generalized to a wide range of nanostructures, such as nanowires and nanoparticles.

Published on 28 June 2010 on http://pubs.rsc.org | doi:10.1039/C0NJ00138D
Downloaded by University of Saskatchewan on 21 October 2010

Introduction

Despite the extensive research on the chemical doping of single-walled carbon nanotubes (SWCNTs),[1–4] the underlying doping mechanism is not completely understood. The main difficulty arises from the complex electronic structures of SWCNTs, which rely strongly on chirality and diameter.[5,6] Chemical doping of SWCNTs involves physisorption or chemisorption due to the different electron affinity between the SWCNT and adsorbates, and more importantly, charge transfer between the adsorbates and SWCNTs.[7–10] Different types of charge carriers are created in SWCNTs by the choice of functional groups in adsorbates.[1–4,7–10] Recently, concepts of the reduction potential, electron affinity, and ionization energy of doping materials were introduced to control the doping level of SWCNTs.[1,11] The reduction potential of a chemical species is defined as its tendency to acquire electrons and be reduced, and the electron affinity is the energy needed to detach an electron from a singly charged negative ion. However, in organic chemistry, they are linearly correlated with each other.[12] The ionization potential is also closely related to the oxidation potential.[13] O'Connell *et al.* reported that the chiral selective reaction of semiconducting SWCNTs relies on the reduction potential of different organic molecules.[11] However, they estimated only semiconducting SWCNTs. Takenobu *et al.* also demonstrated that the controlled amphoteric doping of SWCNTs was strongly dependent on the electron affinity and ionization potential of the dopants.[1]

The absolute electrode potential is the difference in electronic energy between a point inside the metal (Fermi level) of an electrode and a point outside the electrolyte in which the electrode is submerged.[14] The desired definition of the absolute electrode potential of a metal in an aqueous solution is

$$E^{M}_{(abs)} = \frac{\Phi^{M}}{e} + \Delta^{M}_{S}\Psi^{0}_{\sigma=0} \quad (1)$$

$$E^{M}_{(abs)} = E^{M}_{(SHE)} + E^{0}(H^{+}/H_2)_{(abs)}(V) \quad (2)$$

where $E^{M}_{(abs)}$ is the absolute electrode potential of a metal, $E^{M}_{(SHE)}$ denotes the electrode potential of a metal relative to the standard hydrogen electrode (SHE), $E^{0}(H^{+}/H_2)_{(abs)}$ (4.44 ± 0.02 V at 25 °C) is the absolute potential of the SHE in an aqueous solution, Φ^{M} is the work function of metal, e is electron, and $\Delta^{M}_{S}\Psi^{0}_{\sigma=0}$ is the contact potential difference at the metal(M)–solution(S) interface under $\sigma = 0$ the zero charge point condition at the interface. It should be noted that the standard value for the potential difference at the metal–solution interface $\Delta^{M}_{S}\Psi^{0}_{\sigma=0}$ is not measurable due to the nature of the nanosized SWCNT. It also depends on the types of metal, such as mercury (−0.25 V) and silver (+0.72 V), in an aqueous solution.[14] In the present work, it was assumed that the contact potential difference is zero because the absolute electrode potential of various aromatic hydrocarbons, such as anthracene, coronene and perylene, was linearly correlated with the π–π* transition from the highest occupied orbital to the lowest unoccupied molecular orbital, *i.e.*, it approaches the work function of graphite, which has a zero gap.[15] This leads

[a] *BK21 Physics Division, Department of Energy Science, Center for Nanotubes and Nanostructured Composites, Sungkyunkwan University, Suwon 440-746, South Korea. E-mail: leeyoung@skku.edu; Fax: +82 31-290-5954; Tel: +82 31-299-6507*
[b] *Samsung Advanced Institute of Technology, Yongin, Gyeonggi-do, 446-712, South Korea. E-mail: jaeyoung88.choi@samsung.com; Fax: +82 31-280-9349; Tel: +82 31-280-9332*
† Electronic supplementary information (ESI) available: Supporting Fig. S1–S4. See DOI: 10.1039/c0nj00138d

View Online

Published on 28 June 2010 on http://pubs.rsc.org | doi:10.1039/C0NJ00138D
Downloaded by University of Saskatchewan on 21 October 2010

that $\Delta_S^M \Psi_{\sigma=0}^0$ is almost zero gap for carbon nanotubes similar to graphite. From eqn (1) and (2), the following can be obtained:

$$E_{(SHE)}^{M} = \frac{\Phi^{M}}{e} - 4.44\,(V) \qquad (3)$$

The electrode potential relative to the SHE $E_{(SHE)}^{M}$ through the absolute electrode potential is quite useful for understanding the reduction–oxidation reaction between SWCNTs and molecules.

This paper proposes a strategy for controlling the doping types and doping concentrations by choosing the doping material with the appropriate reduction potential relative to SWCNTs. The electrode potentials of the SWCNTs relative to the SHE were extracted based on theoretical calculations. This strategy was demonstrated by choosing several doping materials and further applied to obtain highly conducting transparent SWCNTs.

Experimental

Film preparation

SWCNTs (purity 93 wt%), which were synthesized using an arc discharge method, were purchased from Hanwha Nanotech., Korea. The diameters ranged from 1.2 to 1.8 nm with a mean diameter of 1.5 nm and a typical length of a few μm. SWCNTs (2 mg) were added to 30 ml of 1,2-dichloroethane (DCE: anhydrous, 99.8% Sigma-Adrich) followed by sonication in a bath type sonicator (RK 106, Bandelin Electronic, Berlin, Germany) for 6 h. This solution was centrifuged (Hanil Science Industrial Co., Ltd., Mega 17R) at 10 000 g for 10 min. The supernatant was sprayed onto a quartz substrate (2×2 cm^2) with an Ar gas brush pistol (Gunpiece GP-1, Fuso Seiki Co., Ltd.) and further heat-treated to 600 °C for 30 min under an Ar atmosphere to exclude the other doping effect.[7,8]

Doping procedure

Several doping materials, 2,3-dichloro-5,6-dicyano-*p*-benzoquinone (DDQ: purity 98%, Sigma-Aldrich), nitrosyl tetrafluoroborate ($NOBF_4$: purity 95%, Sigma-Aldrich), and gold(III) chloride ($AuCl_3$: purity 99%, Sigma-Aldrich) with different reduction potentials were chosen carefully to distinguish the doping capability. They were dissolved in nitromethane (Sigma-Aldrich) at different concentrations. One 400 μl drop of the doping solution was placed onto the SWCNT film. After a residual time of 30 s, the solvent was spin-coated at 2500 rpm for 60 s (Midas System, Spin 2000).

Preparation of transparent conducting film

Fifteen milligrams of a dodecylbenzenesulfonic acid sodium salt (NaDDBS: Sigma-Aldrich) as a surfactant was dispersed in 30 ml deionized water and 30 mg SWCNTs was then added followed by sonication in a bath sonicator for 10 h. The solution was centrifuged at 10 000 g for 10 min. The supernatant was sprayed onto a (10×10 cm^2) polyethylene terephthalate (PET) substrate with an Ar gas brush pistol. The PET substrate was kept on the substrate holder at 100 °C. After the spray was terminated, the TCF film was immersed in a HNO_3 (OCI Company Ltd.) solution for one hour to remove the NaDDBS. The film was rinsed in an isopropanol solution several times and immersed in deionized water to neutralize until the pH reached 7. The resulting sample was used for the doping experiment with $AuCl_3$.

Measurement

The optical properties of the SWCNT films after doping were characterized by UV-Vis-NIR absorption spectroscopy (Cary 5000, Varian) and Raman spectroscopy (RM1000-Invia, Renishaw) with a laser excitation energy of 1.96 eV. The sheet resistance of the samples was obtained from four probe measurements (Keithely 2000). The surface morphology of the film was observed by FE-SEM (JSM700F, JEOL). The formation of Au particles after doping was characterized by XPS (Physical Electronics, Quantum 2000) using focused monochromatized AlKα radiation (1486.6 eV).

Results and discussion

Redox potential of SWCNT

The redox potential of SWCNT relative to the SHE $E_{(SHE)}^{SWCNT}$ is strongly chirality- and diameter-dependent. This was determined based on theoretical calculations. From eqn (3), the reduction potential can be extracted from the work function of the SWCNTs. The work function of the metallic and semiconducting SWCNTs was determined from density functional calculations within the generalized gradient approximation (GGA).[16] The redox potential of metallic tubes (E_F^M) and the first occupied van Hove singularities (vHs) of the semiconducting tubes (V_{1s}) (or the Fermi level of semiconducting tube) were determined from GGA using eqn (3).[5] The redox potential (V) of the corresponding vHs was fitted using the following equation,

$$E_{(SHE)}^{SWCNT}(V) = \frac{a}{d_t(\mathrm{nm})} + b \qquad (4)$$

where a and b are the fitting parameters and d_t is the diameter of a nanotube. The values for E_F^M and V_{1s} are listed in Table 1. Since even GGA does not generate an accurate band gap, the first occupied vHs (V_{1s}) and unoccupied vHs (C_{1s}) of the semiconducting SWCNTs were obtained from fluorescent spectroscopy.[17] Combining those with the Fermi level determined from theory, the rest of the occupied and unoccupied states were fitted using a similar (n,m) argument of a tight binding scheme.[5] Table 1 lists the parameters for the plot.

Fig. 1 shows the redox potential plot of the SWCNTs with a wide range of diameters and chiralities. Below the Fermi level are the filled states of the first and second vHs of

Table 1 Data fitting of the redox potential of SWCNT. ($V = a/d_t$ (nm) + b)[a]

	E_F^M	V_{1m}	C_{1m}	E_F^S	V_{1s}	C_{1s}	V_{2s}	C_{2s}
a	−0.105	0.825	−1.034	0.112	0.442	−0.198	0.732	−0.507
b	0.396	0.827	−0.034	0.119	0.263	−0.024	0.407	−0.168

[a] $V_{i\alpha}$ ($C_{i\alpha}$) indicates filled (empty) ith level or oxidation (reduction) potential. α stands for semiconducting (s) and metallic (m) nanotubes.

 This journal is © The Royal Society of Chemistry and the Centre National de la Recherche Scientifique 2010

View Online

Published on 28 June 2010 on http://pubs.rsc.org | doi:10.1039/C0NJ00138D
Downloaded by University of Saskatchewan on 21 October 2010

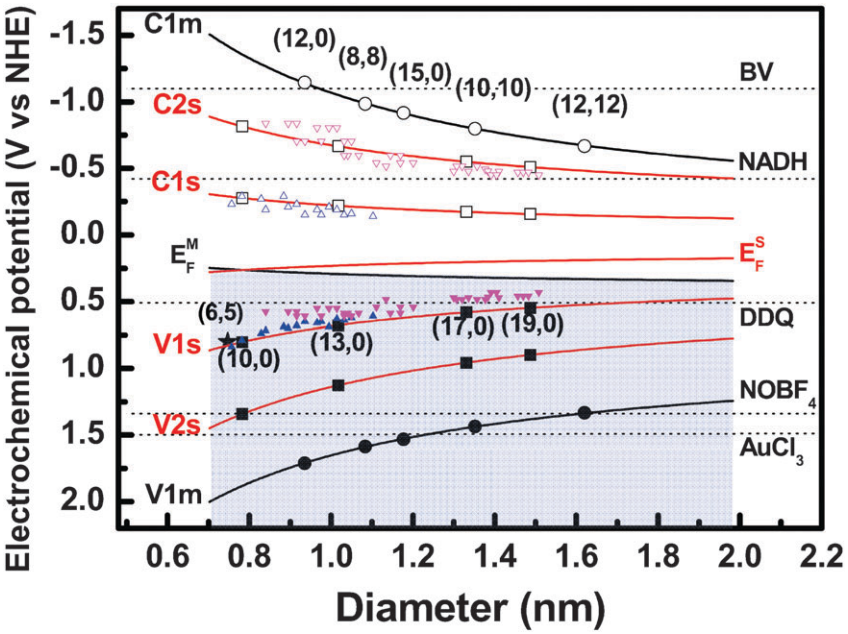

Fig. 1 Redox potential of various nanotubes as a function of the diameter. The values in parentheses indicate the chiral index of the SWCNTs. The reduction potentials of dopants are also provided as dotted lines. $V_{i\alpha}$ ($C_{i\alpha}$) indicates the filled (empty) ith level. α stands for semiconducting (s) and metallic (m) nanotubes. The triangle and reverse triangle indicate the experimental redox potentials of SWCNT from ref. 19 and 20, respectively.

semiconducting nanotubes and metallic nanotubes. Similar plots can be also drawn for empty states. The V_{is} and C_{is} indicate the oxidation potential and reduction potential of the SWCNT from ith energy level, respectively. The previously observed V_{1s} of the (6,5) tube (800 mV) is in good agreement with our plot.[18] More recently, the redox potentials of SWCNTs were measured by electrochemistry with photoluminescence and optical absorption spectroscopy.[19,20] The results from Tanaka *et al.* indicated by the triangle in Fig. 1 coincide with our theoretical results.[19] However, the reduction potentials of SWCNTs from Paolucci *et al.* indicated by the reversed triangle in Fig. 1 were much lower than those of our prediction.[20] These discrepancies were attributed to the initial n-doping medium by Na or K, where the Fermi level of SWCNTs is already upshifted to some degree.

It should be emphasized that both experiments measured the redox potentials of semiconducting SWCNTs only. However, our theory predicts the redox potentials of not only semiconducting SWCNTs but also metallic SWCNTs. The reduction potentials of the chosen doping materials are also provided in the plot. For example, the Au^{3+} ion has the largest reduction potential of 1.50 V among others and is even larger than V_{1s} and V_{2s} of the semiconducting nanotubes independent of the diameter and the V_{1m} of the metallic ones in the large diameter region.[21] Other dopants in organic medium, such as DDQ of 0.51 V and NO^+ ion of 1.34 V, are also electron-withdrawing groups but the degree of electron extraction will depend on the chirality and diameter.[22,23]

Doping effect in the optical absorption and Raman spectra

In order to demonstrate this concept, the sample was characterized by absorption spectroscopy and Raman spectroscopy after doping with various dopants. The equilibrium state of the dopant was first checked with different concentrations. The pristine sample clearly shows the absorption due to vHs transitions of the semiconducting (E_{11}^S and E_{22}^S) and metallic (E_{11}^M) nanotubes. The peak intensity of particularly E_{11}^S decreased with increasing DDQ concentration but no further appreciable changes were observed at a high doping concentration of 80 mM (Fig. 2a). This suggests that the doping level was saturated in the equilibrium state. The peak intensity of E_{11}^S in Fig. 2a was reduced but not quenched completely, even at a high DDQ concentration. This is expected because the redox potential of DDQ is lower than those of the first vHs in the valence band for most diameter ranges in the sample. Similar experiments were carried out for $NOBF_4$ in Fig. 2b. At low $NOBF_4$ concentration, the E_{11}^S began to disappear, and had disappeared completely at high concentrations but E_{22}^S peak was upshifted slightly. The disappearance of the E_{11}^S peak was attributed to the depletion of electrons from the first vHs in the valence band, as predicted from Fig. 1, i.*e.*, no electron is available to show absorption. The upshift of the E_{22}^S peak indicates electron depletion at the larger diameter SWCNTs due to the larger relative difference in the redox potential between the SWCNTs and NO^+ ion.

Fig. 3 shows the absorption and Raman spectra of the selected concentration (or maximum concentration) which were in equilibrium at different dopants. In the case of 80 mM Au^{3+} ion doping, all peaks, regardless of semiconducting or metallic nanotubes, had disappeared, as shown in Fig. 3a. This is similar to that observed with the redox potential plot in that Au^{3+} has a larger reduction potential of 1.50 V than the SWCNTs with up to the second filled levels over a wide range of diameters, as shown in Fig. 1. The peak

View Online

Published on 28 June 2010 on http://pubs.rsc.org | doi:10.1039/C0NJ00138D
Downloaded by University of Saskatchewan on 21 October 2010

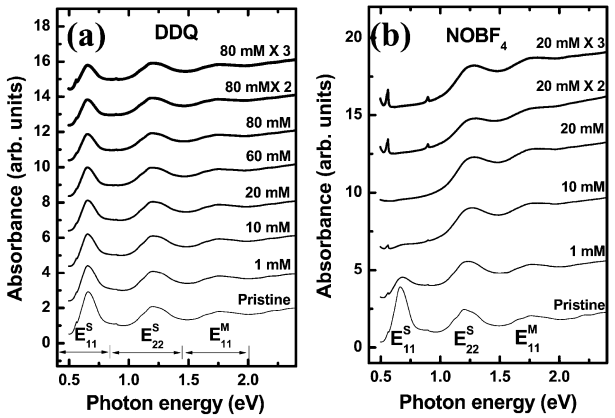

Fig. 2 Optical absorption spectra of SWCNTs doped with (a) DDQ and (b) $NOBF_4$ in nitromethane as a function of the mole concentration. The doping experiment was carried out using a spin-casting method.

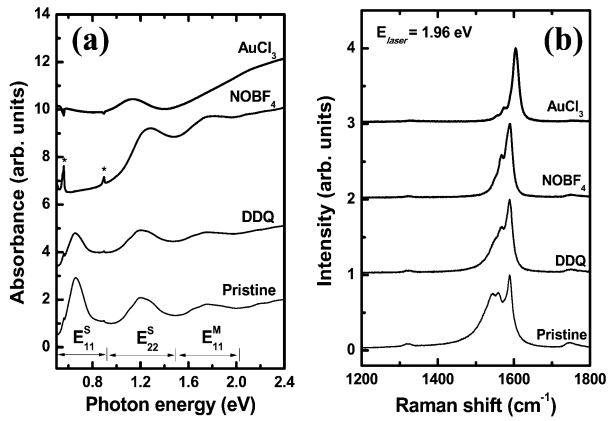

Fig. 3 Absorption spectra (a) and G-band of Raman spectra at a laser energy of 1.96 eV (b) from the samples doped with various dopants of DDQ, $NOBF_4$, and $AuCl_3$ in the equilibrium state. The asterisk indicates the absorption from the quartz substrate.

near 1.1 eV was downshifted considerably compared to the E_{22}^S peak and was defined as a new peak, independent of the peaks of the pristine sample. This can be attributed to a new transition from a deeper level to the newly empty states due to charge depletion, where the strict selection rule no longer applies.[14] The morphology and charge-transfer phenomena were further confirmed by field-emission scanning electron microscopy (FE-SEM) and X-ray photoelectron spectroscopy (XPS), respectively. The gold particles were visible on the SWCNT surface (Fig. S1 and S2, ESI†). The other dopants did not form aggregates. From the XPS measurements, it was confirmed that the Au^{3+} ion was reduced to Au^0 by charge-transfer during the doping procedure (Fig. S3, ESI†).

Charge depletion (or charge transfer) was also observed by Raman spectroscopy with an excitation energy of 1.96 eV. Fig. 3b shows the G-band with a clear metallic contribution in the low energy region in the pristine sample due to strong electron–phonon interactions.[6,24] The G-band was fitted with six components similar to the previous report (not shown here).[7,24] This contribution was reduced systematically with increasing reduction potential. In the case of $AuCl_3$, the long tail component had disappeared completely. This was also correlated with the quenching of E_{11}^M in the optical absorption spectra in Fig. 3a. On the other hand, the G^+ peak position at around 1590 cm^{-1} was also upshifted by approximately 10 cm^{-1}, particularly in the case of Au^{3+} ion doping. These alterations were attributed to charge extraction from the SWCNTs to the doping material and the related phonon stiffening.[3,8]

Change of the sheet resistance by doping

For proof of concept, the sheet resistance was measured after p-doping, *i.e.*, extraction of electrons from SWCNTs increases the hole carrier concentration and the sheet resistance is expected to decrease. The changes in the Schottky barrier due to a Fermi level shift could be another reason for the decrease in resistance.[25] Table 2 shows the change in sheet resistance.

The sheet resistance of three films was reduced consistently compared to that of the pristine sample. Although the decrease in sheet resistance is remarkable in the case of Au^{3+} ions, similar changes in the sheet resistance were also observed in the case of NO^+ ions. In previous work,[25] although the work function increased consistently up to 4.73 eV as a function of the Au^{3+} ion concentration, the change in sheet resistance was limited to approximately 90% at more than 60 mM of $AuCl_3$. Therefore, it was concluded that the change in sheet resistance in the case of NO^+ ions was similar to that of the sheet resistance after Au^{3+} ion doping. On the other hand, gold particles could modify the conductivity of SWCNT film as an interconnect between the SWCNT bundles. Nevertheless, since the change in sheet resistance due to Au^{3+} ion doping compared to NO^+ ions doping is similar, it is believed that the bridging effect does not enhance the conductivity of the SWCNT film appreciably. Furthermore, only few gold particles were observed on the SWCNT film surface (Fig. S1, ESI†). For practical applications, Au^{3+} ions were chosen to observe the effect of doping on a transparent conducting film. The SWCNTs were dispersed using a sodium dodecylbenzenesulfonate (NaDDBS) surfactant in deionized water. The SWCNT solution was sprayed on a polyethylene naphthalate (PEN) film. The doping solvent was then spin-casted onto the SWCNT film similar to previous work.[26] Fig. 4 shows the change in sheet resistance *vs.* transmittance. The sheet resistance of the pristine sample was reduced consistently independently of the film thickness or transmittance by approximately 50% after removing the surfactant using an acid treatment. Subsequent Au^{3+} doping reduced the sheet resistance by a further 30%. The change in the transmittance was negligible with doping.

Table 2 Change in sheet resistance after doping with different concentrations

	1 mM	10 mM	20 mM	60 mM	Remark
DDQ	64%	66%	65%	67%	
$NOBF_4$	80%	89%	90%	92%[a]	
$AuCl_3$	56%	60%	73%	93%	Ref. 25

[a] Two drops of 20 mM were used in the 60 mM sample due to the low solubility of $NOBF_4$ in nitromethane.

 This journal is © The Royal Society of Chemistry and the Centre National de la Recherche Scientifique 2010

View Online

Published on 28 June 2010 on http://pubs.rsc.org | doi:10.1039/C0NJ00138D
Downloaded by University of Saskatchewan on 21 October 2010

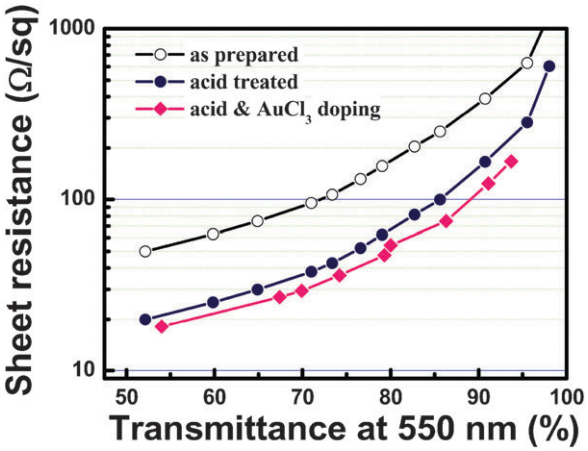

Fig. 4 The sheet resistance of acid-treated samples and those followed by $AuCl_3$ treatment in terms of the transmittance at 550 nm. The sheet resistance reached 100 Ω sq^{-1} at 90% transmittance.

The small sheet resistance with doping meets the technical criteria for electrode applications. For example, a sheet resistance of 100 Ω sq^{-1} at 90% transmittance is a good candidate for touch panels, and a material with a sheet resistance of 50 Ω sq^{-1} at 80% transmittance would be suitable for a common electrode in large size displays.

Absorption strength dependence on the choice of solvent

The absorption strength also relies on the choice of solvent. SWCNTs should be dispersed well to accommodate the dopants easily. A polar solvent with a too high dielectric constant, such as water, suppresses the dispersion of SWCNTs and charge transfer due to the large screening effect by the solvent medium. For example, the SWCNTs in water alone are not well dispersed and 80 mM $NOBF_4$ doping in water was not very efficient, as shown in Fig. 5a. On the other hand, SWCNTs were relatively well dispersed in *N*-methyl-2-pyrrolidone (NMP), and $NOBF_4$ was soluble in NMP. Nevertheless, doping was not very effective, as shown in Fig. 5b. This suggests that the combination between dopant and solvent

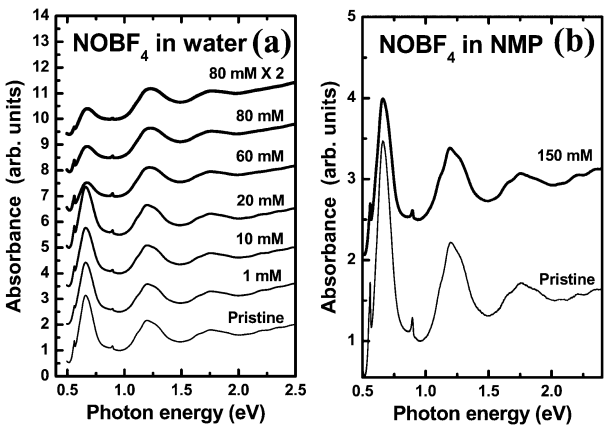

Fig. 5 Optical absorption spectra of the SWCNTs doped with $NOBF_4$ prepared in (a) water and (b) NMP. Compared to the nitromethane solvent, the E_{11}^S transition was not reduced significantly.

such as salvation-free energy of ions in the solvent and absolute free energy of the solvent should be matched well to maximize the doping efficiency.[15,27,28] The π-plasmon peak located near 4.5 eV was not changed appreciably even with doping (Fig. S4, ESI†). Although the background absorbance near the infra-red and visible range might be altered slightly, the variance in the vHs transitions discussed in the current study should not be affected by the changes in background absorbance.

Conclusions

The degree of nanotube doping can be determined by the redox potential of the dopant in its equilibrium state. The redox potential plot of the SWCNTs was constructed based on theoretical calculations. The redox potential argument was demonstrated by choosing several dopants with different redox potentials. In addition to the redox potential, in order to maximize the doping effect, care should be taken when choosing the solvent types and counterion to the dopant. The strategy of p-type doping can also be applied to n-type doping. A n-type dopant has a higher negative reduction potential, as indicated in Fig. 1. In this case, the electrons from n-dopants are donated to the CNTs. The n-dopants of benzyl viologen (BV) and β-nicotinamide adenine dinucleotide (NADH) with a negative reduction potential have been already demonstrated.[29,30] Although this doping effect can be applied to obtain highly conducting CNT films, the same principle can be applied to many other systems involving control of the dopant types and doping concentrations to obtain high-speed transistors. Furthermore this concept can be generalized to nanowires and nanoparticles by constructing a similar redox potential plot.

Acknowledgements

This study was supported financially by MEST through the STAR-faculty project, the WCU program through MEST (R31-2008-000-10029-0), and Industrial Technology Development Program (10031734) of MKE, Korea.

References

1 T. Takenobu, T. Kambara, N. Akima, T. Takahashi, M. Shiraishi, K. Tsukagoshi, H. Kataura, Y. Aoyagi and Y. Iwasa, *Adv. Mater.*, 2005, **17**, 2430.
2 T. Takenobu, T. Takano, M. Shiraishi, Y. Murakami, M. Ata, H. Kataura, Y. Achiba and Y. Iwasa, *Nat. Mater.*, 2003, **2**, 683.
3 A. M. Rao, P. C. Eklund, S. Bandow, A. Thess and R. E. Smalley, *Nature*, 1997, **388**, 257.
4 M. Shim, A. Javey, N. W. Kam and H. Dai, *J. Am. Chem. Soc.*, 2001, **123**, 11512.
5 K. H. An and Y. H. Lee, *Nano*, 2006, **1**, 115.
6 M. S. Dresselhaus, G. Dresselhaus, R. Saito and A. Jorio, *Phys. Rep.*, 2005, **409**, 47.
7 H.-J. Shin, S. M. Kim, S.-M. Yoon, A. Benayad, K. K. Kim, S. J. Kim, H. K. Park, J.-Y. Choi and Y. H. Lee, *J. Am. Chem. Soc.*, 2008, **130**, 2062.
8 R. Voggu, C. S. Rout, A. D. Franklin, T. S. Fisher and C. N. R. Rao, *J. Phys. Chem. C*, 2008, **112**, 13053.
9 M. S. Strano, C. A. Dyke, M. L. Usrey, P. W. Barone, M. J. Allen, H. Shan, C. Kittrell, R. H. Hauge, J. M. Tour and R. E. Smalley, *Science*, 2003, **301**, 1519.

View Online

10 J. Chen, M. A. Hamon, H. Hu, Y. Chen, A. M. Rao, P. C. Eklund and R. C. Haddon, *Science*, 1998, **282**, 95.
11 M. J. O'Connell, E. E. Eibergen and S. K. Doorn, *Nat. Mater.*, 2005, **4**, 412.
12 L. D. Hicks, A. J. Fry and V. C. Kurzweil, *Electrochim. Acta*, 2004, **50**, 1039.
13 S. Janietz, D. D. C. Bradley, M. Grell, G. Giebeler, M. Inbasekaran and E. P. Woo, *Appl. Phys. Lett.*, 1998, **73**, 2453.
14 S. Trasatti, *Pure Appl. Chem.*, 1986, **58**, 955.
15 A. Matsuda, R. Notoya and H. Hiratsuka, *J. Res. Inst. Catal., Hokkaido Univ.*, 1980, **28**, 269.
16 J. Zhao, J. Han and J. P. Lu, *Phys. Rev. B: Condens. Matter Mater. Phys.*, 2002, **65**, 193401.
17 R. B. Weisman and S. M. Bachilo, *Nano Lett.*, 2003, **3**, 1235.
18 M. Zheng and B. A. Diner, *J. Am. Chem. Soc.*, 2004, **126**, 15490.
19 Y. Tanaka, Y. Hirana, Y. Niidome, K. Kato, S. Saito and N. Nakashima, *Angew. Chem., Int. Ed.*, 2009, **48**, 7655.
20 D. Paolucci, M. M. Franco, M. Iurlo, M. Marcaccio, M. Prato, F. Zerbetto, A. Pénicaud and F. Paolucci, *J. Am. Chem. Soc.*, 2008, **130**, 7393.
21 *CRC Handbook of Chemistry and Physics*, ed. D. R. Lide, CRC Press, 89th edn, 2008–2009.
22 J.-L. Ciprelli, C. Clarisse and D. Delabouglise, *Synth. Met.*, 1995, **74**, 217.
23 K. Y. Lee, D. J. Kuchynka and J. K. Kochi, *Inorg. Chem.*, 1990, **29**, 4196.
24 S. D. M. Brown, A. Jorio, P. Corio, M. S. Dresselhaus, G. Dresselhus, R. Saito and K. Kneipp, *Phys. Rev. B: Condens. Matter Mater. Phys.*, 2001, **63**, 155414.
25 K. K. Kim, J. J. Bae, H. K. Park, S. M. Kim, H.-Z. Geng, K. A. Park, H.-J. Shin, S.-M. Yoon, A. Benzyad, J.-Y. Choi and Y. H. Lee, *J. Am. Chem. Soc.*, 2008, **130**, 12757.
26 H.-Z. Geng, K. K. Kim, K. P. So, Y. S. Lee, Y. Chang and Y. H. Lee, *J. Am. Chem. Soc.*, 2007, **129**, 7758.
27 R. Gomer and G. Tryson, *J. Chem. Phys.*, 1977, **66**, 4413.
28 C. P. Kelly, C. J. Cramer and D. G. Truhlar, *J. Phys. Chem. B*, 2007, **111**, 408.
29 S. M. Kim, J. H. Jang, K. K. Kim, H. K. Park, J. J. Bae, W. J. Yu, I. H. Lee, G. Kim, D. D. Loc, U. J. Kim, E.-H. Lee, H.-J. Shin, J.-Y. Choi and Y. H. Lee, *J. Am. Chem. Soc.*, 2009, **131**, 327.
30 B. R. Kang, W. J. Yu, K. K. Kim, H. K. Park, S. M. Kim, Y. Park, G. Kim, H.-J. Shin, U. J. Kim, E.-H. Lee, J.-Y. Choi and Y. H. Lee, *Adv. Funct. Mater.*, 2009, **19**, 1.

Published on 28 June 2010 on http://pubs.rsc.org | doi:10.1039/C0NJ00138D
Downloaded by University of Saskatchewan on 21 October 2010

 This journal is © The Royal Society of Chemistry and the Centre National de la Recherche Scientifique 2010